Facile preparation of 3D GO with caffeic acid for efficient adsorption of norfloxacin and ketoprofen

Ying Lu, Youlin Li, Yi Gao, BoXuan Ai, Wei Gao and Guilong Peng

ABSTRACT

In this paper, a simple and green method was developed to fabricate a three-dimensional (3D) graphene-based material with the assistance of caffeic acid (CA). The prepared 3D graphene displayed fast and high sorption for norfloxacin (NOR) and ketoprofen (KP). Their adsorption equilibrium was achieved within 12 h for NOR and KP, which was attributed to their fast diffusion in the porous structure of the 3D graphene. The maximum adsorbed amount of this adsorbent was 220.99 mg/g for NOR and 125.37 mg/g for KP according to the Langmuir model at pH 6.6, 298 K. In the competitive adsorption of six pharmaceuticals, the organic compounds in the form of cations are preferentially adsorbed on the adsorbent. The co-existing organic compounds in the actual wastewater do not seriously inhibit the adsorption of NOR and KP. This study provides the theoretical basis for the facile and low-cost preparation of high-performance 3D graphene adsorbents. The results of this study demonstrate the potential utility of 3D graphene as a very effective adsorbent for pharmaceuticals removal from contaminated water.

Key words | ketoprofen, norfloxacin, sorption, three-dimensional graphene

Ying Lu
Guilong Peng (corresponding author)
State Key Laboratory of Silkworm Genome Biology, Key Laboratory of Sericultural Biology and Genetic Breeding, Ministry of Agriculture and Rural Affairs, College of Biotechnology,
Southwest University,
Chongqing 400715, China
E-mail: *pengguilong0325@163.com*

Ying Lu
Department of Mathematics and Physics,
Officers College of PAP,
Chengdu 610213, China

Youlin Li
Yi Gao
School of Chemistry and Chemical Engineering,
Southwest University,
Chongqing 400715, China

BoXuan Ai
School of Environment, Beijing Key Laboratory for Emerging Organic Contaminants Control, State Key Joint Laboratory of Environment Simulation and Pollution Control (SKLESPC),
Tsinghua University,
Beijing 100084, China

Wei Gao
Department of Pharmacy,
The Affiliated Hospital of Zunyi Medical University,
Zunyi 563000, China

HIGHLIGHTS

- 3D graphene is prepared by the self-assembly of reduced graphene oxide.
- 3D graphene has high adsorption capacity for pharmaceuticals.
- Maximum adsorption capacity of the prepared 3D graphene was 220.99 mg/g for NOR and 125.37 mg/g for KP, respectively.

INTRODUCTION

With the rapid industrial development of modern society, environmental pollution, especially water pollution, has become a worldwide threat of growing concern. Among these pollutants, pharmaceuticals and personal care products (PPCPs) have received widespread attention as emerging pollutants due to their possible threats to the water environment and human health (Liu & Wong 2013). PPCPs can enter aquatic environments through multiple pathways, including domestic wastewater, hospital discharges, improper manufacturing disposal, sewage treatment plants (STPs), and water treatment plants (WTPs) (Leung *et al.* 2012; Liu & Wong 2013). In recent years, the pollution of surface water and groundwater from PPCPs has become a serious problem (Bulloch *et al.* 2015; Huang *et al.* 2016; Bhatnagar & Anastopoulos 2017; Song & Jhung 2017). Therefore, it is necessary to develop effective methods to remove PPCPs in the water environment.

Three-dimensional (3D) graphene-based materials with tuned surface properties have received extensive attention in catalysis, energy conversion, and environmental applications (Geim & Novoselov 2007; Dong *et al.* 2012b; Novoselov *et al.* 2012). Especially, as absorbents, monolithic graphene aerogels consisting of 3D porous frameworks can provide multidimensional adsorption sites, which greatly improve absorption efficiency (Chen *et al.* 2011a; Wu *et al.* 2015). Recently, a variety of methods have been developed

doi: 10.2166/wst.2020.193

for fabrication of 3D graphene, such as chemical vapor deposition (CVD) (Fan *et al.* 2010; Chen *et al.* 2011b), hydrothermal treatment (Song *et al.* 2016; Mu *et al.* 2017), in situ reducing self-assembly (Zhang *et al.* 2012; Liu *et al.* 2017), and the cross-linking method (Worsley *et al.* 2010). In the CVD method, 3D nickel foams are usually used as substrates, onto which graphene is deposited under high-temperature conditions (700–900 °C) and harsh atmospheric conditions, which is thus of high cost (Chen *et al.* 2011b; Dong *et al.* 2012a). Hydrothermal processes under high temperature (180–200 °C) and pressure are an effective method to fabricate 3D graphene, which was first reported by Shi and his co-workers, and the hydrogels have excellent mechanical and electrical properties (Xu *et al.* 2010a). However, the size and high-pressure requirements of the hydrothermal reactor (Teflon-lined autoclave) greatly limit its large-scale production. It is still difficult to prepare 3D architectures of graphene in the absence of chemical or physical cross-linkers (Chen & Yan 2011).

Recently, graphene self-assembly assisted by chemical reductants has been realized under mild synthesis conditions and low instrument requirements. Self-assembly is usually carried out under low-temperature heating below 100 °C, without stirring or vigorous hydrothermal processes. In this strategy, graphene oxide (GO) is reduced in the presence of a reducing agent, and the in situ reduced graphene sheets can be spontaneously assembled into 3D graphene-structured thermally reduced GO sheets through π–π interactions (Xu *et al.* 2010a). However, some poisonous chemicals, such as metal ions, hydrazine (N_2H_4), $NaBH_4$, Na_2S and HI have often been used (Chen *et al.* 2011a; Cong *et al.* 2012), which are unfriendly to the environment. There are also some biocompatible molecules such as vitamin C (Sui *et al.* 2011), dopamine (Gao *et al.* 2013), amino acids (Zhang *et al.* 2015), DNA (Xu *et al.* 2010b), and other phenols (e.g., gallic acid, tannin acid, and tea polyphenol) (Lei *et al.* 2011; Wang *et al.* 2011; Li *et al.* 2013; Luo *et al.* 2016) that have been used to fabricate 3D graphene materials. These biomolecules are relatively expensive, thus greatly increasing the production cost.

Caffeic acid (CA, 3,4-dihydroxycinnamic acid, $C_9H_8O_4$) is one of the most important hydroxycinnamic acids in phenolic compounds and is widely available in plants and foods (Chen & Ho 1997; Gülçin 2006). Previous studies have shown that CA has a strong antioxidant capacity due to the presence of hydroxyl groups at positions 3 and 4, and it can be used as a mild reducing agent for GO (Bo *et al.* 2014), promoting the self-assembly of reduced graphene oxide (RGO) into 3D structures. Here, we devote the work to prepare 3D structures of graphene via a green, mild, and low-cost method, which is based on the chemical reduction and in situ self-assembly of GO. Two typical PPCPs, norfloxacin (NOR) and ketoprofen (KP), were selected as the main target contaminants to evaluate the adsorption performance of the prepared 3D graphene, and the underlying adsorption mechanism was also studied. The results showed that 3D graphene hydrogel exhibited high removal efficiency for NOR and KP from water, and satisfactory results were obtained from competitive adsorption in both simulated solution and actual wastewater, thus it can be used as an efficient adsorbent in water purification, and its derivatives can broaden the potential application in wastewater treatment.

MATERIALS AND METHODS

Materials

Graphene oxide (GO, purity >98%, layers <3) was purchased from Chengdu Organic Chemicals Co., Ltd, Chinese Academy of Science (Chengdu, China). CA, NOR, KP, benzene, 1-naphthylamine, 1-methylnaphthalene, 5-amino-1-naphthol, naproxen (NP), bisphenol A (BPA), ofloxacin (OF) and ciprofloxacin (CIP) were purchased from Aladdin Ltd (Shanghai, China) and their physicochemical properties are listed in Table S1 in the Supporting Information. Other chemicals were bought from Sinopharm Chemical Reagent Co., Ltd (Shanghai, China). All chemicals were of analytical grade and used as received without further purification. Ultrapure water was used throughout all experiments, and produced by a Milli-Q system (Millipore, USA). Wastewater was collected from a large-scale wastewater treatment plant (Beijing, China). The primary characteristics of the wastewater are shown in Table S2, and the HPLC–MS/MS chromatograms of PPCPs are illustrated in Figure S1.

Preparation of 3D graphene architectures

The GO sheets (2 mg/mL) were dispersed in aqueous solution with a sonifier (Scientz-IID, Φ6, 30% amplitude, 950 W/20 kHz) for 30 min, and used as a stock of GO suspension. CA (10 mg/mL) was dispersed in ethanol by ultrasonication to form a homogeneous dispersion. Then, equal volume (5 mL) aqueous solutions of GO and 200 μL of CA were mixed to form homogeneous solutions and the mixtures were heated at 85 °C in a water-bath for 8 h under atmospheric pressure without stirring. Finally, the obtained black 3D graphene hydrogel (Figure S2) was

washed thoroughly with water and then freeze-dried to obtain the 3D CA-RGO xerogels.

Characterization

Scanning electron microscopy (SEM) experiments were performed with a field emission scanning electron microscope (JSM-7800 F & TEAM Octane Plus, JEOL, Japan). X-ray diffraction (XRD) patterns were obtained by an X-ray diffractometer (Rigaku S2, Japan) employing Cu Kα as source of radiation. X-ray photoelectron spectra (XPS) were recorded from an X-ray photoelectron spectrometer (ESCALAB 250Xi, USA). The Fourier transform infrared (FT-IR) spectrum was obtained with a Tensor 27 spectrometer (Bruker Co., Germany). Raman spectra were conducted with a Raman spectrometer (HR-800, Horiba, France) with 514 nm laser excitation. Surface electrical properties of the materials were determined with a zeta-potential instrument (Delsa Nano C, Beckman Coulter, USA). The Brunauer–Emmett–Teller (BET) surface area and pore size distribution were analyzed by an automated gas sorption analyzer (Quantachrome, autosorb-iQ, USA).

Sorption experiments

Sorption experiments were conducted at 25 °C in an orbital shaker at 130 rpm with 10 mg of adsorbent in glass conical flasks containing 50 mL of solution except for evaluating the sorption kinetics experiments. In the investigation of sorption kinetics of NOR and KP, their initial concentrations were 20 mg/L (pH 6.6). In the sorption isotherm experiments, the initial concentrations of NOR and KP were in the range of 10–80 mg/L (pH 6.6), and the sorption time was 24 h. In the pH-effect experiments, the initial solution pH ranged from 3.0 to 10.0, and the adsorbates were fixed at 20 mg/L. After the adsorption experiments, the samples were filtered through a 0.22 μm nylon membrane. All sorption experiments were conducted in duplicate, and the mean values were adopted. The concentrations of the targets were determined with a UV–vis spectrophotometer (Cary 100, USA) and high-performance liquid chromatograph (HPLC). The HPLC analysis was performed using a UFLC Shimadzu system (Shimadzu, Kyoto, Japan), consisting of two LC-20AD pumps, DGU-20A3 degasser, SPD-M20A photodiode array (PDA, D2&W, 190–800 nm) detector, CBM-20A controller and CTO-10AS thermostat. The separations were performed on an Agilent TC-C18 column (5 μm 250 × 4.6 mm).

RESULTS AND DISCUSSION

Optimization of the amount of CA

The effect of the amount of CA on the adsorption of NOR and KP onto the 3D CA-RGO is shown in Figure S3 (Supporting Information). The adsorbed amounts (q_e) of NOR and KP on the 3D CA-RGO decreased with increasing the amount of CA. When the amount of CA was too low (below 50 μL), it could not effectively induce the formation of 3D graphene hydrogel. An amount of CA as low as 150 μL could induce the formation of 3D graphene hydrogel; however, the obtained black monolith was not very compact. But further increasing the amount of CA led to the adsorbed amounts (q_e) of NOR and KP decreasing sharply. Thus, 200 μL of CA (mass ratio of CA:GO of 1:5) was used to prepare the 3D CA-RGO for the following experiments.

Characterization of 3D CA-RGO

SEM images are used to reveal the microscopic morphology of the as-prepared 3D CA-RGO. As can be seen (Figure 1(a)), GO has a typical sheet-like structure with some wrinkles, and the 3D CA-RGO has an interconnected 3D porous network structure with pore sizes ranging from several hundred nanometers to several micrometers, which are assembled by the randomly oriented and wrinkled GO nanosheets (Figure 1(b)). The FT-IR spectra of GO and 3D CA-RGO are shown in Figure S4. There are several absorption bands at 3,431, 1,734, 1,632, 1,440, and 1,070 cm^{-1} for GO, which are associated with the O-H stretching vibration, C=O stretching vibration, aromatic C=C stretching vibration, O-H deformation vibration, and C-O stretching vibration, respectively. The peak of the 3D CA-RGO pattern decreased significantly, indicating that the oxygen-containing group decreased after the reduction reaction. The Raman spectra of GO and 3D CA-RGO are shown in Figure 1(c). The peaks at 1,340 and 1,590 cm^{-1} are the characteristic peaks of the D-band and G-band, respectively. The D-band shows defects such as disorder, edges and boundaries of the carbon skeleton, while the G-band is caused by tensile vibration of sp^2 hybrid carbon atoms. D-band to G-band strength ratio (ID/IG) is usually used to evaluate the structural disorder and defects of graphite carbon materials. The ID/IG ratio values of GO and 3D CA-RGO are estimated to be 0.848 and 1.016, respectively. The intensity ratio of the ID/IG in the 3D CA-RGO is greater after the chemical reduction compared with that of GO, indicating that the reduction process can cause an increase in disorder.

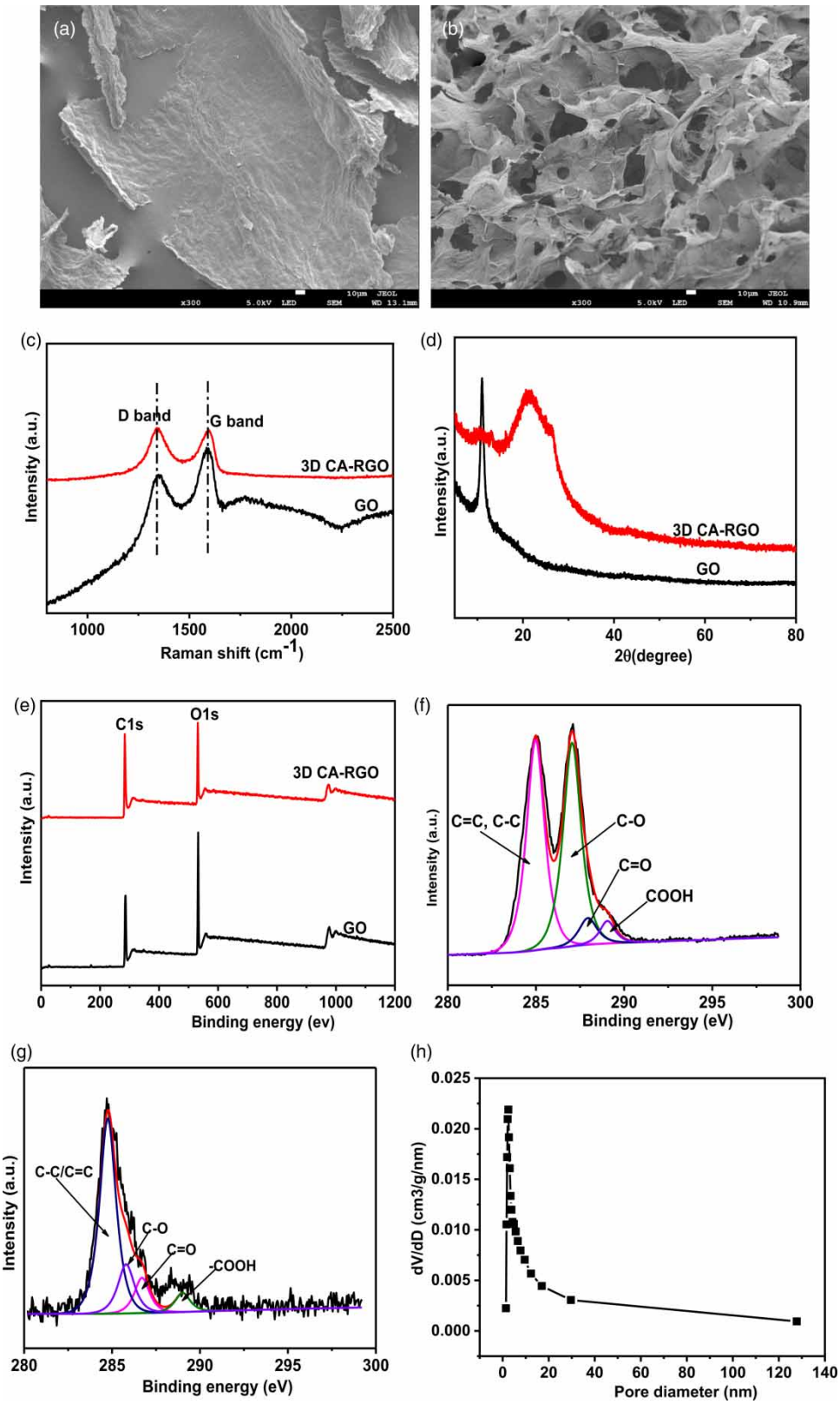

Figure 1 | SEM images of (a) GO and (b) 3D CA-RGO; (c) Raman spectra of GO and 3D CA-RGO; (d) XRD patterns of GO and 3D CA-RGO; and (e) XPS survey spectra of GO and 3D CA-RGO; high-resolution XPS C1s spectra of (f) GO and (g) 3D CA-RGO as well as (h) BJH pore diameter distribution of 3D CA-RGO.

The X-ray diffraction (XRD) spectra of GO and 3D CA-RGO are represented in Figure 1(d). The peak intensity of GO at 11.2° nearly disappeared along with the reaction, while a new broad peak near 22.7° appeared in the 3D CA-RGO, which is attributed to a decrease of the interlayer spacing during the reduction process. Figure 1(e) shows the XPS survey spectra of GO and 3D CA-RGO. After reduction, the content of carbon and oxygen in the 3D CA-RGO was relatively increased and decreased, respectively. The content of oxygen decreased from 31.42% to 24.01%, indicating that a certain amount of the oxygen-containing groups were removed in the reduction process. Figure 1(f) shows the C1s XPS spectra of GO and 3D CA-RGO. For GO, four different peaks centered at 284.6 eV, 287.05 eV, 287.92 eV, and 289.06 eV are detected, which correspond to C=C/C-C in aromatic rings, C–O (epoxy and alkoxy), C=O, and COOH groups, respectively (Sui *et al.* 2011). After reduction by CA, the intensities of the C1s peaks of the carbons binding to oxygen decrease significantly, especially the peak of C–O (286.6 eV) (Figure 1(g)). These results reveal that GO can be efficiently reduced by CA. The N_2 adsorption/desorption isotherm (Figure 1(h)) shows the 3D CA-RGO with a BET specific surface area of 260.3 cm^2/g. The distribution of pore size was computed using the Barrett–Joyner–Halenda (BJH) method, and the total pore volume was calculated to be 0.368 cm^3/g, with the BJH mean pore diameter of 3.9 nm, indicating that a great many mesopores existed in the 3D CA-RGO.

Adsorption kinetics and isotherms

Figure 2(a) shows the sorption kinetics of NOR and KP on the 3D CA-RGO. The adsorption equilibria of NOR and KP were both almost reached within 12 h, and most of the adsorption was accomplished in the first few hours. To further investigate the sorption kinetics of NOR and KP, the pseudo-second-order model was used to describe the adsorption kinetic data of NOR and KP on the 3D CA-RGO, and the modeling results are shown in Table S3. The initial adsorption rate (v_0) of NOR was 164.60 mg/g/h, much higher than that of KP (61.30 mg/g/h), and the equilibrium adsorbed amounts (q_e) of NOR on the adsorbent were much higher than those of KP. This may be attributed to electrostatic attraction and hydrogen bonding between NOR and the 3D CA-RGO. The norfloxacin molecule contains fluorine atoms and nitrogen atoms, which can form more hydrogen bonds, thus it is more favorable for the adsorption of NOR.

The sorption isotherms of NOR and KP on the 3D CA-RGO and their fitting results by the Langmuir and Freundlich models are shown in Figure 2(b), and the fitting results are presented in Table S4. The adsorption isotherms of NOR and KP on the 3D CA-RGO were described better by the Langmuir model than the Freundlich model, according to their correlation coefficients (R^2). The maximum sorption capacities (q_m) of NOR and KP on the 3D CA-RGO were 220.99 and 125.37 mg/g, respectively. This difference can be attributed to different adsorption mechanisms. At pH 6.6, the KP ($pK_a = 4.45$) was negatively charged, and the surface charge of the 3D CA-RGO (Figure S5) was negative, thus the electrostatic repulsion existing between the adsorbent and KP led to its lower sorption capacities. Actually, the π–π interaction should play a major role in the adsorption of KP onto the 3D CA-RGO.

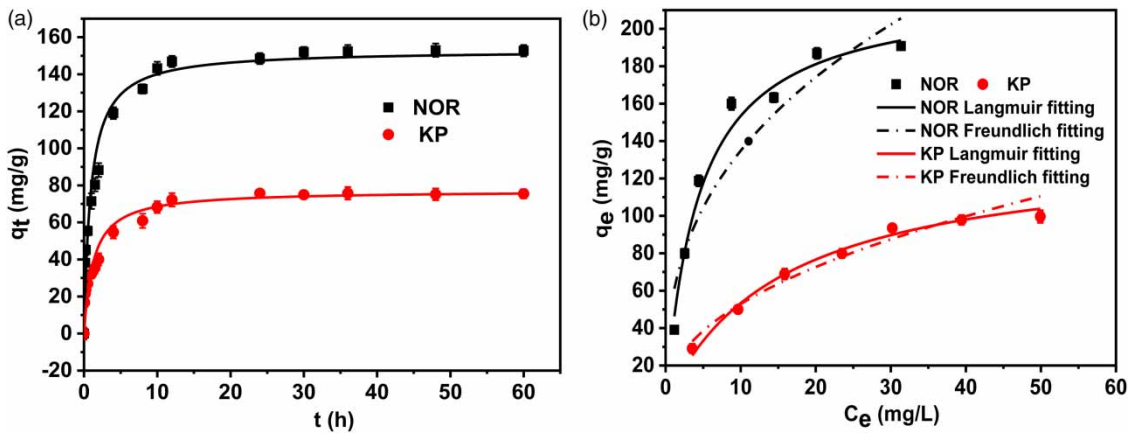

Figure 2 | (a) Sorption kinetics of NOR and KP on 3D CA-RGO and fitting results using the pseudo-second-order equation, as well as (b) their sorption isotherms and modeling fits by the Freundlich and Langmuir equations.

Effect of pH

The effect of solution pH on the adsorption of NOR and KP is presented in Figure 3. There was no obvious change in the adsorption of NOR with the increase of solution pH ranging from 3.0 to 8.0, but it began to decrease with further increase of the initial pH. When the pH is higher than 5, the adsorption of KP decreases rapidly, especially when the pH >9. The zeta potentials are all negative values in the pH 3–10 range (Figure S5). Thus, the 3D CA-RGO adsorbent is negatively charged in the entire environmentally relevant pH range, which is more conducive to the adsorption of positively charged cations. NOR has two pK_a values of 6.22 and 8.51, and it can exist in cationic form (NOR^+), zwitterionic ($NOR^\pm$) and neutral form (NOR^0), or anionic form (NOR^-) depending on the solution pH (Figure S6). In the adsorption process, electrostatic attraction is suggested to play an important role, and the high amount of NOR sorption on 3D CA-RGO was steady in the initial pH range 3.0–8.0. When the pH was higher than 8, the anionic form (NOR^-) increased, resulting in a significant decrease in its adsorption capacity. The pK_a value of KP is 4.45, the negative KP species increased at pH above 5, and the electrostatic repulsion increased with increasing solution pH, leading to the decrease of KP when pH increased from 5.0 to 10.0. The electrostatic repulsion between KP and 3D CA-RGO led to the low adsorption capacity.

Competitive adsorption

Co-existing compounds significantly affect the adsorption of target compounds on adsorbents (Du *et al.* 2015). In the investigation of competitive adsorption of different pharmaceuticals, 10 mg of adsorbent was added into 50 mL of 20 mg/L single and mixed pharmaceuticals solutions. The adsorbed amounts of NOR, KP, NP, BPA, OF and CIP on the 3D CA-RGO were compared (Figure 4(a)). NOR, OF and CIP in the single-solute system exhibited higher adsorption capacity than KP, NP and BPA. All the target compounds in the single-solute system exhibited substantially higher adsorption capacity than those in the mixed six-solute system. Since the pK_a values of KP and NP are 4.45 and 4.2, they exist as anions at pH above 5.0, and electrostatic repulsion prevented the adsorption of KP and NP on the 3D CA-RGO, leading to the lower adsorption capacity of KP and NP. Thus, π–π interactions should play a dominant role in the sorption process for KP and NP. The higher removal percentages of NP and NOR than KP and BPA were also observed in the actual wastewater, suggesting that electrostatic interaction also plays an important role in the actual wastewater. It is worth noting that other organic pollutants can also be completely removed with the increasing of the 3D CA-RGO. Additionally, the adsorbed amounts of KP and NOR on the four adsorbents GAC, PAC, GO and 3D CA-RGO were compared (Figure 4(b)), and the surface area as well as pore volume of GAC and PAC are provided in Table S5. The 3D CA-RGO exhibited the highest adsorption capacity (148.9 mg/g for NOR and 72.5 mg/g for KP, respectively) among the four adsorbents. Also, the GO showed good adsorption performance; nevertheless, it was extremely hydrophilic, and so was hard to separate from water. The GAC showed the lowest adsorption capacity of 51.6 mg/g for NOR, and 30.3 mg/g for KP, respectively. As one of the most widely used commercial adsorbents, PAC was considered to be a reliable adsorbent for removing organic substances due to its strong adsorption performance (Zhou *et al.* 2020). We can observe the results that the adsorption capacity of 3D CA-RGO for NOR is still higher than that of PAC (112.3 mg/g). Although the adsorption capacity of 3D CA-RGO for KP was not as good as that of PAC, it still has the potential to be used as an efficient adsorbent for PPCP removal in the water environment.

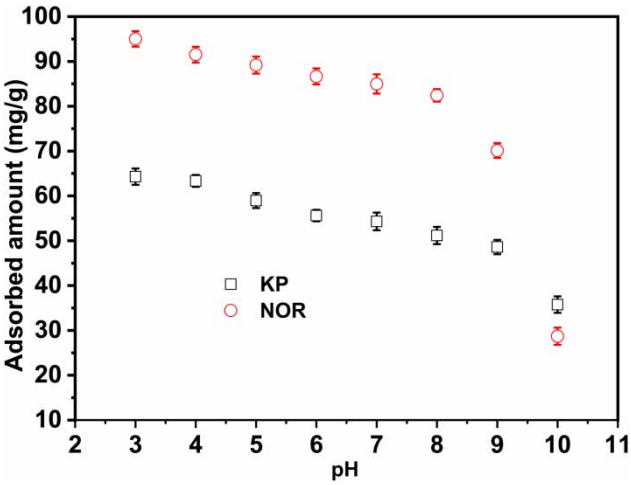

Figure 3 | Effect of solution pH on NOR and KP adsorption.

Adsorption thermodynamics

The influence of temperature on the adsorption of NOR and KP by 3D CA-RGO was investigated. Additional adsorption experiments for NOR and KP were conducted at 313 and 333 K (Figure S7), respectively. The thermodynamic parameters were calculated from the following equations

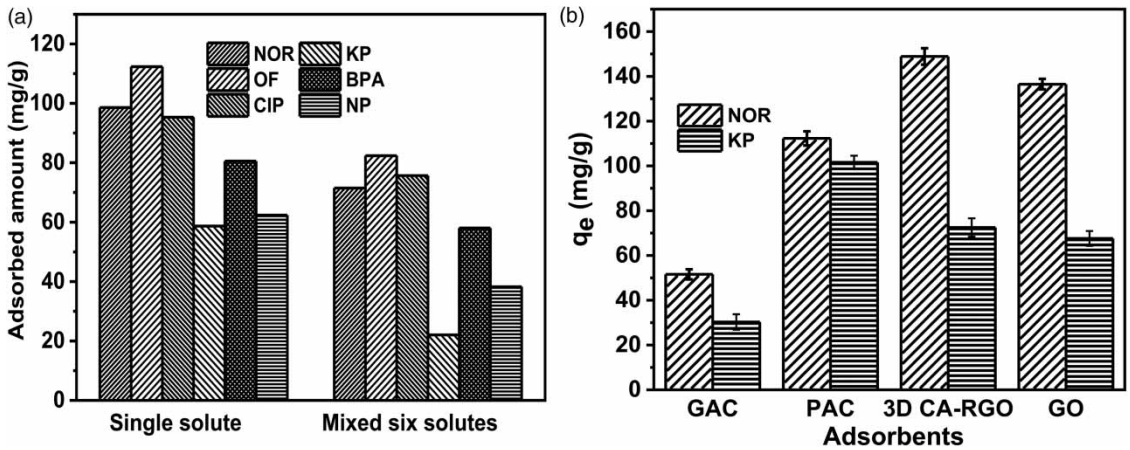

Figure 4 | (a) Adsorption of NOR by 3D CA-RGO in the single and mixed PPCPs solutions as well as (b) adsorbed amounts of NOR and KP on different adsorbents.

(Zhang *et al.* 2011):

$$\ln K^0 = \frac{\triangle S^0}{R} - \frac{\triangle H^0}{RT} \quad (1)$$

$$K_c = \frac{q_e}{C_e} \quad (2)$$

$$\triangle G^0 = -RT \ln K_c \quad (3)$$

where K_c is the distribution coefficient, R is the universal gas constant (8.314 J mol^{-1} K^{-1}), T is temperature in kelvin, ΔS^0 (J mol^{-1} K^{-1}), ΔH^0 (kJ mol^{-1}), and ΔG^0 (kJ mol^{-1}) are the changes in entropy, enthalpy, and Gibbs free energy, respectively, q_e (mg/g) is the amount of target compounds absorbed onto the adsorbent at equilibrium, and C_e (mg/L) is the equilibrium concentration of target compounds. The values of adsorption equilibrium constant ($\ln K^0$) are obtained by plotting $\ln K_c$ versus C_e and extrapolating C_e to zero, and the value of the intercept is the value of $\ln K^0$. The distribution coefficients for NOR and KP at 293, 313, and 333 K are shown in Figure 5. Values of $\ln K^0$ obtained by plotting $\ln K_c$ versus C_e are 3.207 (293 K), 3.502 (313 K), 3.80 (333 K) for NOR and 1.966 (293 K), 2.177 (313 K), 2.322 (333 K) for KP, respectively. ΔS^0 and ΔH^0 were calculated using the slope and intercept of plots of $\ln K^0$ against $1/T$ (Figure S8). The obtained thermodynamic parameters are presented in Table 1. The negative values of ΔG^0 indicate that the adsorption is a spontaneous process, and the value of ΔG^0 becomes more negative with the increase of temperature, suggesting that the adsorption process is more favorable at higher temperature due to the dehydration of NOR and KP. The obtained positive ΔH^0 value suggests an endothermic adsorption mechanism, which is supported by the results that the adsorption of NOR and KP on the 3D CA-RGO increase with increasing temperature.

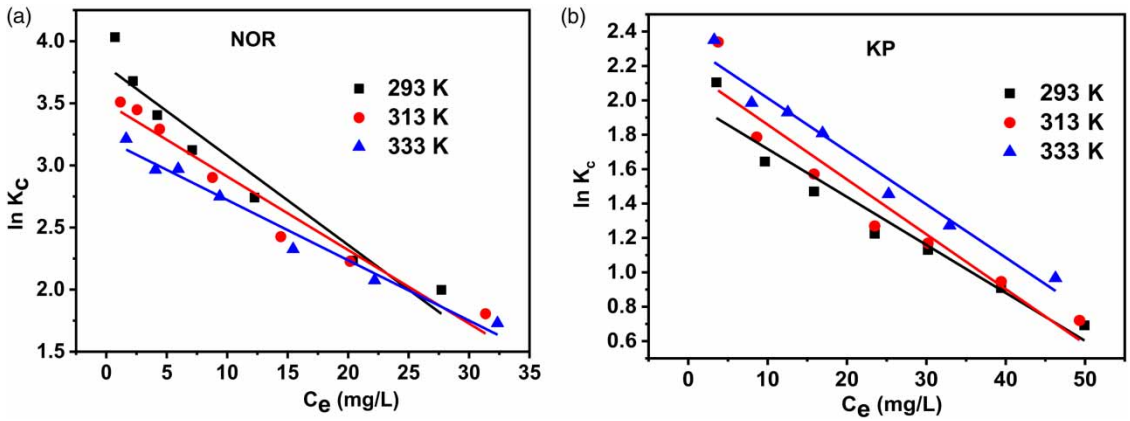

Figure 5 | Linear plots of ln K_c vs C_e at 293, 313, 333 K.

Table 1 | Thermodynamic parameters for the adsorption of NOR and KP onto the 3D CA-RGO at different temperatures

Adsorbates	ΔH^0(kJ mol^{-1})	ΔS^0(J mol^{-1} K^{-1})	ΔG^0(kJ mol^{-1})		
			293 K	313 K	333 K
NOR	3.96	23.03	−2.90	−3.45	−3.71
KP	3.54	17.71	−1.73	−2.00	−2.35

Adsorption mechanism

Based on the characteristics of NOR and KP, the adsorption mechanisms may involve electrostatic interaction, π–π interaction, and hydrogen bonding. In view of the above results, in the single pharmaceutical solutions, the adsorbed amounts of NOR, OF and CIP are higher than those of KP, NP and BPA, the adsorption capacity for BPA is higher than those of KP and NP, and the electrostatic interaction during the adsorption process can be considered to play an important role. According to the pK_a (Table S1) of the six compounds, NOR, OF and CIP are zwitterionic forms at the tested solution pH (6.6), KP and NP are in the form of anionic species, and BPA is in its molecular form. As a consequence, electrostatic attraction for NOR, OF, and CIP and electrostatic repulsion for KP and NP can occur in the adsorption process, and there is no electrostatic interaction occuring between BPA and adsorbent. In order to explain π–π interaction and hydrogen bonding also playing an important role between the organic compounds and the 3D CA-RGO surface, the 3D CA-RGO was used to remove different organic compounds including benzene, 1-methylnaphthalene, 1-naphthylamine and 5-amino-1-naphthol. The q_e values (Figure 6) were increased in the order of benzene <1-methylnaphthalene <1-naphthylamine <5-amino-1-naphthol. The 1-methylnaphthalene has two benzene rings, thus the π–π interaction is stronger between the 3D CA-RGO and 1-methylnaphthalene than benzene with one benzene ring, 5-amino-1-naphthol with -NH_2 and -OH groups, or 1-naphthylamine with -NH_2 groups. Therefore, the H-bonding can be explained by H-donation from the 3D CA-RGO (with -OH groups) and H-acceptance between 1-naphthylamine and 5-amino-1-naphthol (mainly O and N atoms). The sorption capacity for 5-amino-1-naphthol is better than that for 1-naphthylamine, and this result confirms that the number of H-bonding is very important in the relative adsorption performance. So, it is reasonable that the 3D CA-RGO has much higher adsorbed amounts for 5-amino-1-naphthol than the other three compounds.

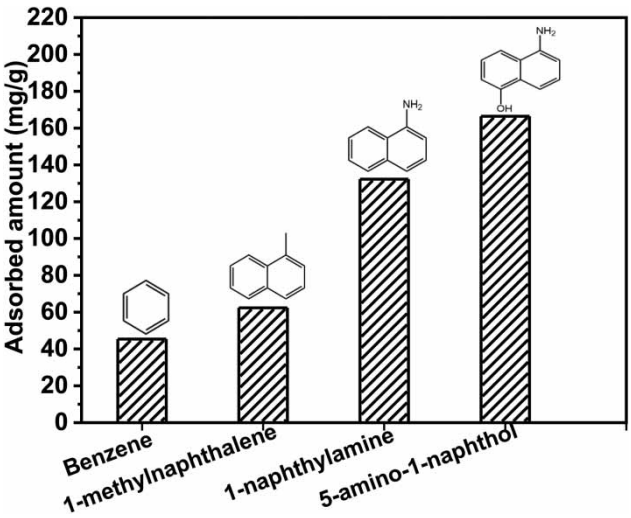

Figure 6 | Adsorbed amounts of different organic compounds on the 3D CA-RGO.

Regeneration and reuse of 3D CA-RGO

The experiments of 3D CA-RGO regeneration and reuse were conducted to investigate the reusability of 3D CA-RGO. Figure S9 shows the adsorbed amounts of NOR and KP on the 3D CA-RGO after five times of washing regeneration with methanol, and the detailed experimental method is described in the Supporting Information. It can be seen that the desorption percentage of both NOR and KP increased with increasing the volume of methanol, and nearly 100% was achieved after the volume of methanol was 15 mL (Figure S9(a)). As can be seen from Figure S9(b), the results exhibited steady sorption for NOR and KP in five cycles, showing high reusability, so the adsorbent can be used repeatedly for the adsorption of pharmaceuticals.

CONCLUSIONS

In summary, we report a simple, environmentally friendly, and economical method for the synthesis of a 3D RGO with CA as both reducing agent and physical cross-linking sites. We have reported the first example of the application

of 3D CA-RGO as an efficient sorbent for adsorption of NOR and KP from water and real wastewater, and it exhibited high adsorption capacities and recycling performance toward NOR and KP. The results showed that the adsorption performance was related to the properties of adsorbent and adsorbates. Both electrostatic interaction and π–π interaction played important roles during the adsorption process. The coexisting organic compounds had no obvious interference with NOR and KP sorption on the 3D CA-RGO, which also had good adsorption capacity in the complex organic wastewater. The results show that 3D CA-RGO has a strong potential to become an efficient and green adsorbent for hazardous organic compounds with applications in actual industrial wastewater. The processes to fabricate 3D RGO are facile, low-cost, and can be scalable to industrial levels.

ACKNOWLEDGEMENTS

We thank the Fundamental Research Funds for the Central Universities (SWU119058) and (XDJK2018C043) for financial support.

SUPPLEMENTARY MATERIAL

The Supplementary Material for this paper is available online at https://dx.doi.org/10.2166//wst.2020.193.

REFERENCES

Bhatnagar, A. & Anastopoulos, I. 2017 Adsorptive removal of bisphenol A (BPA) from aqueous solution: a review. *Chemosphere* **168**, 885–902.

Bo, Z., Shuai, X., Mao, S., Yang, H., Qian, J., Chen, J., Yan, J. & Cen, K. 2014 Green preparation of reduced graphene oxide for sensing and energy storage applications. *Scientific Reports* **4**, 4684.

Bulloch, D. N., Nelson, E. D., Carr, S. A., Wissman, C. R., Armstrong, J. L., Schlenk, D. & Larive, C. K. 2015 Occurrence of halogenated transformation products of selected pharmaceuticals and personal care products in secondary and tertiary treated wastewaters from southern California. *Environmental Science & Technology* **49** (4), 2044–2051.

Chen, J. H. & Ho, C.-T. 1997 Antioxidant activities of caffeic acid and its related hydroxycinnamic acid compounds. *Journal of Agricultural and Food Chemistry* **45** (7), 2374–2378.

Chen, W. & Yan, L. 2011 *In situ* self-assembly of mild chemical reduction graphene for three-dimensional architectures. *Nanoscale* **3** (8), 3132–3137.

Chen, W., Li, S., Chen, C. & Yan, L. 2011a Self-assembly and embedding of nanoparticles by in situ reduced graphene for preparation of a 3D graphene/nanoparticle aerogel. *Advanced Materials* **23** (47), 5679–5683.

Chen, Z., Ren, W., Gao, L., Liu, B., Pei, S. & Cheng, H.-M. 2011b Three-dimensional flexible and conductive interconnected graphene networks grown by chemical vapour deposition. *Nature Materials* **10**, 424–428.

Cong, H.-P., Ren, X.-C., Wang, P. & Yu, S.-H. 2012 Macroscopic multifunctional graphene-based hydrogels and aerogels by a metal ion induced self-assembly process. *ACS Nano* **6** (3), 2693–2703.

Dong, X.-C., Xu, H., Wang, X.-W., Huang, Y.-X., Chan-Park, M. B., Zhang, H., Wang, L.-H., Huang, W. & Chen, P. 2012a 3D graphene–cobalt oxide electrode for high-performance supercapacitor and enzymeless glucose detection. *ACS Nano* **6** (4), 3206–3213.

Dong, X., Chen, J., Ma, Y., Wang, J., Chan-Park, M. B., Liu, X., Wang, L., Huang, W. & Chen, P. 2012b Superhydrophobic and superoleophilic hybrid foam of graphene and carbon nanotube for selective removal of oils or organic solvents from the surface of water. *Chemical Communications* **48** (86), 10660–10662.

Du, Z., Deng, S., Chen, Y., Wang, B., Huang, J., Wang, Y. & Yu, G. 2015 Removal of perfluorinated carboxylates from washing wastewater of perfluorooctanesulfonyl fluoride using activated carbons and resins. *Journal of Hazardous Materials* **286**, 136–143.

Fan, Z., Yan, J., Zhi, L., Zhang, Q., Wei, T., Feng, J., Zhang, M., Qian, W. & Wei, F. 2010 A three-dimensional carbon nanotube/graphene sandwich and its application as electrode in supercapacitors. *Advanced Materials* **22** (33), 3723–3728.

Gao, H., Sun, Y., Zhou, J., Xu, R. & Duan, H. 2013 Mussel-inspired synthesis of polydopamine-functionalized graphene hydrogel as reusable adsorbents for water purification. *ACS Applied Materials & Interfaces* **5** (2), 425–432.

Geim, A. K. & Novoselov, K. S. 2007 The rise of graphene. *Nature Materials* **6**, 183–191.

Gülçin, İ. 2006 Antioxidant activity of caffeic acid (3,4-dihydroxycinnamic acid). *Toxicology* **217** (2–3), 213–220.

Huang, B., Xiong, D., Zhao, T. T., He, H. & Pan, X. J. 2016 Adsorptive removal of PPCPs by biomorphic HAP templated from cotton. *Water Science and Technology* **74** (1), 276–286.

Lei, Y., Tang, Z., Liao, R. & Guo, B. 2011 Hydrolysable tannin as environmentally friendly reducer and stabilizer for graphene oxide. *Green Chemistry* **13** (7), 1655–1658.

Leung, H. W., Minh, T. B., Murphy, M. B., Lam, J. C. W., So, M. K., Martin, M., Lam, P. K. S. & Richardson, B. J. 2012 Distribution, fate and risk assessment of antibiotics in sewage treatment plants in Hong Kong, South China. *Environment International* **42**, 1–9.

Li, J., Xiao, G., Chen, C., Li, R. & Yan, D. 2013 Superior dispersions of reduced graphene oxide synthesized by using gallic acid as a reductant and stabilizer. *Journal of Materials Chemistry A* **1** (4), 1481–1487.

Liu, J.-L. & Wong, M.-H. 2013 Pharmaceuticals and personal care products (PPCPs): a review on environmental contamination in China. *Environment International* **59**, 208–224.

Liu, C., Liu, H., Xu, A., Tang, K., Huang, Y. & Lu, C. 2017 In situ reduced and assembled three-dimensional graphene aerogel for efficient dye removal. *Journal of Alloys and Compounds* **714**, 522–529.

Luo, J., Lai, J., Zhang, N., Liu, Y., Liu, R. & Liu, X. 2016 Tannic acid induced self-assembly of three-dimensional graphene with good adsorption and antibacterial properties. *ACS Sustainable Chemistry & Engineering* **4** (3), 1404–1413.

Mu, W., Yu, Q., Hu, R., Li, X., Wei, H. & Jian, Y. 2017 Porous three-dimensional reduced graphene oxide merged with WO_3 for efficient removal of radioactive strontium. *Applied Surface Science* **423**, 1203–1211.

Novoselov, K. S., Fal'ko, V. I., Colombo, L., Gellert, P. R., Schwab, M. G. & Kim, K. 2012 A roadmap for graphene. *Nature* **490**, 192–200.

Song, J. Y. & Jhung, S. H. 2017 Adsorption of pharmaceuticals and personal care products over metal–organic frameworks functionalized with hydroxyl groups: quantitative analyses of H-bonding in adsorption. *Chemical Engineering Journal* **322**, 366–374.

Song, X., Chen, Y., Rong, M., Xie, Z., Zhao, T., Wang, Y., Chen, X. & Wolfbeis, O. S. 2016 A phytic acid induced super-amphiphilic multifunctional 3D graphene-based foam. *Angewandte Chemie International Edition* **55** (12), 3936–3941.

Sui, Z., Zhang, X., Lei, Y. & Luo, Y. 2011 Easy and green synthesis of reduced graphite oxide-based hydrogels. *Carbon* **49** (13), 4314–4321.

Wang, Y., Shi, Z. & Yin, J. 2011 Facile synthesis of soluble graphene via a green reduction of graphene oxide in tea solution and its biocomposites. *ACS Applied Materials & Interfaces* **3** (4), 1127–1133.

Worsley, M. A., Pauzauskie, P. J., Olson, T. Y., Biener, J., Satcher Jr, J. H. & Baumann, T. F. 2010 Synthesis of graphene aerogel with high electrical conductivity. *Journal of the American Chemical Society* **132** (40), 14067–14069.

Wu, S., Zhang, K., Wang, X., Jia, Y., Sun, B., Luo, T., Meng, F., Jin, Z., Lin, D., Shen, W., Kong, L. & Liu, J. 2015 Enhanced adsorption of cadmium ions by 3D sulfonated reduced graphene oxide. *Chemical Engineering Journal* **262**, 1292–1302.

Xu, Y., Sheng, K., Li, C. & Shi, G. 2010a Self-assembled graphene hydrogel via a one-step hydrothermal process. *ACS Nano* **4** (7), 4324–4330.

Xu, Y., Wu, Q., Sun, Y., Bai, H. & Shi, G. 2010b Three-dimensional self-assembly of graphene oxide and DNA into multifunctional hydrogels. *ACS Nano* **4** (12), 7358–7362.

Zhang, L., Song, X., Liu, X., Yang, L., Pan, F. & Lv, J. 2011 Studies on the removal of tetracycline by multi-walled carbon nanotubes. *Chemical Engineering Journal* **178**, 26–33.

Zhang, L., Chen, G., Hedhili, M. N., Zhang, H. & Wang, P. 2012 Three-dimensional assemblies of graphene prepared by a novel chemical reduction-induced self-assembly method. *Nanoscale* **4** (22), 7038–7045.

Zhang, X., Liu, D., Yang, L., Zhou, L. & You, T. 2015 Self-assembled three-dimensional graphene-based materials for dye adsorption and catalysis. *Journal of Materials Chemistry A* **3** (18), 10031–10037.

Zhou, J., Ma, F. & Guo, H. 2020 Adsorption behavior of tetracycline from aqueous solution on ferroferric oxide nanoparticles assisted powdered activated carbon. *Chemical Engineering Journal* **384**, 123290.

First received 17 February 2020; accepted in revised form 14 April 2020. Available online 24 April 2020